Dose Painting with a Variable Collimator for the Small Animal Radiation Research Platform (SARRP)

Nathan B. Cho[1], John Wong[2], and Peter Kazanzides[1]

[1] Department of Computer Science, Johns Hopkins University, Baltimore MD, USA
[2] Department of Radiation Oncology, Johns Hopkins Medical Institution, Baltimore MD, USA

Abstract. The goal of radiation treatment is to irradiate cancer cells (i.e., a target region) without destroying adjacent healthy tissue. Thus, it is advantageous to form the beam so that it best approximates the target, thereby reducing the amount of dose absorbed in critical regions outside the target area. While multi-leaf collimators are common in human clinical systems, small animal radiotherapy systems are typically limited to a set of fixed-size collimators. For these systems, dose painting can be used for conformal dose delivery, but is significantly slower than a multi-leaf collimator. As a compromise solution, a variable rectangular collimator has been developed for the Small Animal Radiation Research Platform (SARRP). This enables more efficient dose painting via the decomposition of a 2D target region into a minimum number of rectangles of variable size, which is the topic of this paper. The proposed method consists of several distinct steps and was implemented on the SARRP Treatment Planning System (TPS).

1 Introduction

One of the major limitations in radiotherapy treatment is undesirable irradiation of the healthy tissue. Many organs, such as the spinal cord, are vulnerable to radiation and should be considered during the treatment planning. In general, the goal of treatment planning is to deliver a tumoricidal dose to a target volume while minimizing the dose absorbed in healthy tissue and critical structures [2]. When optimizing a treatment plan, minimizing the total treatment time is an important factor because it quantifies the efficiency of treatment delivery. Clinical radiotherapy systems often include a multi-leaf collimator (MLC) that can be shaped to best fit the target area and efficiently deliver the radiation dose. In contrast, small animal radiotherapy systems are typically limited to fixed-size cylindrical and rectangular collimators that must be manually installed. This leads to the use of dose painting procedures that move a single collimator (usually cylindrical) through a series of points to cover the target area. For example, dose painting with a fixed-size collimator has been demonstrated on both the Xstrahl SARRP[9] and the PXI X-RAD 225Cx[12]. This technique presents a tradeoff

between the fit to the target area and the delivery time – smaller collimators produce a better fit, but increase the delivery time. Although total beam time can be reduced by switching collimators (e.g., using a large collimator for the interior and a small collimator for the edges), the time to manually change collimators must be considered.

While it is mechanically challenging to construct a MLC for small animal radiotherapy, some compromise solutions are possible. One example is the variable aperture collimator (iris) reported by Graves et al.[6]. This collimator was used with a micro-CT scanner that had been modified to also deliver therapeutic radiation doses. A more recent example is a variable rectangular collimator (see Fig. 1) that has been developed for the Small Animal Radiation Research Platform (SARRP). SARRP is a system for micro-irradiation with on-board cone-beam computed tomography (CBCT) guidance [13]. It includes a Treatment Planning System (TPS) [3] that is based on the open-source 3D Slicer package[10]. The SARRP TPS uses a graphics processing unit (GPU)-accelerated superposition-convolution dose computation method [8] that enables fast dose computation. The availability of a variable rectangular collimator presents an opportunity for significantly reducing the delivery time of dose painting procedures. While several strategies are possible, this paper focuses on algorithms for decomposing an arbitrary 2D target region into a minimum number of rectangles of variable size. This method is implemented on the SARRP TPS.

Fig. 1. Motorized Variable Collimator for SARRP

2 Methods

The proposed method can be achieved by a series of steps: segmentation, simplification, and decomposition. The segmentation step converts a raw image to a label map. This is done using the existing segmentation tools in 3D Slicer. Then, the label map is approximated by a rectilinear polygon in the simplification step. The quality of the fit is determined by a user-selectable grid size. Finally, the rectilinear polygon is decomposed into the minimum number of rectangles in the rectangle fitting step. These steps are illustrated in Fig.2. The rest of this section explains the details of the simplification and decomposition steps.

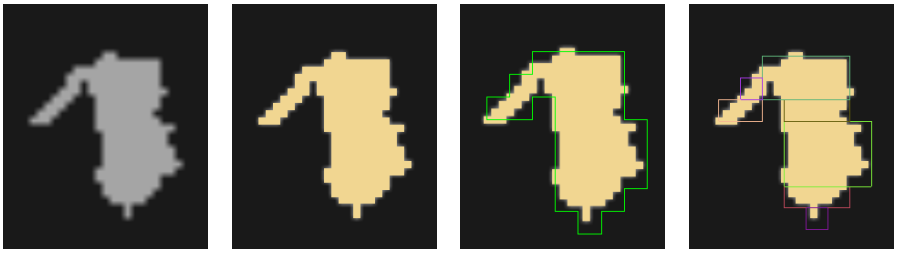

(a) Raw image (b) Segmentation (c) Simplification (d) Decomposition

Fig. 2. High-level workflow of the proposed method.

2.1 Simplification

The simplification step takes the segmented label map (i.e., target area) as input and produces a rectilinear polygon that approximates this area. This can be expressed as the problem of finding an isothetic cover. In this paper, we focus on an outer isothetic cover (OIC), which is the smallest polygon that fully encompasses the target area but may also include some non-target areas. It is also possible to create an inner isothetic cover, which is the largest polygon that contains only the target area (i.e., some parts of the target may be outside the polygon).

We consider that the resolution of the label map is given by the CBCT voxel size, which for SARRP may be as low as 0.2 mm along each dimension. It is not practical or necessary to deliver dose at this resolution. In fact, the smallest collimator currently available for SARRP is 0.5 mm in diameter and this collimator is rarely used due to its low dose rate. Thus, we chose to modify the OIC algorithm described by Biswas et al.[1] to allow less strict coverage of the boundary. This algorithm defines a grid size for the rectilinear polygon – a larger grid size tends to produce a polygon with fewer vertices. In order to construct an outer cover, its combinatorial approach considers the arrangement of grid lines with respect to any pixel (voxel) occupancy at each quadrant while traversing

from the starting point, determining the direction for the next vertex based on the previous decision (e.g., if the previous direction leading to the current point was top to bottom, the next one at the point should not be bottom to top), and finishing when it goes back to the starting point. The range difference to check a pixel occupancy between the original algorithm and our modified algorithm is illustrated in Fig. 3 when the grid size is 6. Essentially, our modification ignores pixels on the boundary of each quadrant and only considers the interior pixels.

In addition, due to the difference of index direction in the SARRP TPS, the first part of the algorithm determining the starting point of OIC was also modified as follows:

$$i_s = \left\lceil \frac{i_0}{g} \right\rceil \times g, \quad j_s = (\left\lfloor \frac{j_0}{g} \right\rfloor + 1) \times g \tag{1}$$

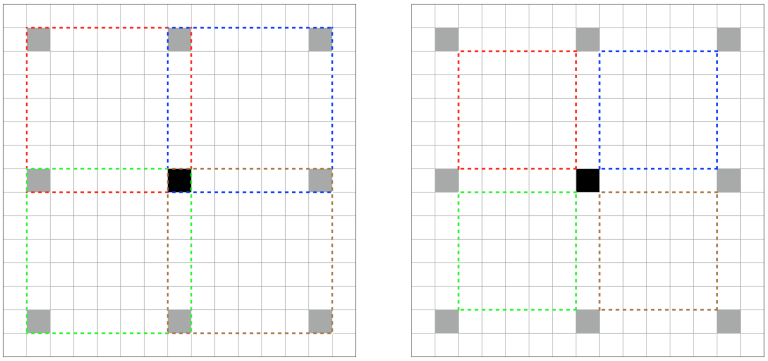

(a) Range of original algorithm (b) Range of modified algorithm

Fig. 3. Four neighboring quadrants for the center pixel (in black) when the grid size is 6. The regions to check pixel occupancy for the 1st, 2nd, 3rd, and 4th quadrants are depicted as dotted lines in blue, red, green, and brown, respectively, in (a) the original algorithm and (b) the modified algorithm. Note that the modified algorithm ignores pixels on the quadrant boundaries.

2.2 Decomposition (Rectangle Fitting)

Once the outer cover is determined, the next step is to decompose it into the minimum number of disjoint sets of rectangles. The idea uses the properties of a bipartite graph to find a minimum order rectangular partition. In other words, the partitioning problem is the same as finding the maximum number of independent vertices in a bipartite graph. As described by Ferrari et al.[4], the polygon decomposition with the minimum number of rectangles can be found by building an intersection graph of horizontal/vertical effective chords, which is a connection between two concave vertices whose x- (i.e., vertical) or y- (i.e., horizontal)

coordinates are the same. It is known that finding the maximum independent set in a general graph is an NP-hard problem. However, in the special case of a bipartite graph, the König-Egerváry theorem states that the maximum matching problem is equivalent to the minimum vertex cover problem, and the Hopcroft-Karp algorithm [7] can be used to find the maximum cardinality matching in polynomial time.

After the dissection with effective chords, there may still be some polygons with concave vertices. For those regions, the polygon to rectangle (PTR) algorithm [5] is applied to further sub-divide each polygon.

3 Implementation and Workflow

The series of steps described in the Methods section was implemented on the SARRP TPS. A synthetic 3D target volume based on a mouse brain image acquired by SARRP was generated with a resolution of 0.2 mm^3. A label map was created using a threshold-based segmentation (i.e., ThresholdEffect) in the Editor module in 3D Slicer.

The TPS includes a slider bar (QSlider) that adjusts the OIC grid size from 2 to 10. For a grid size of 2, the original OIC algorithm is used because the modified algorithm would only check one pixel and would therefore be less robust than the original algorithm which checks nine pixels. The modified algorithm is used for grid sizes greater than 2. The computed OIC is displayed as a MRML model in the 3D Slicer views. Figure 4(a) shows an OIC, with a grid size of 3, represented by green lines.

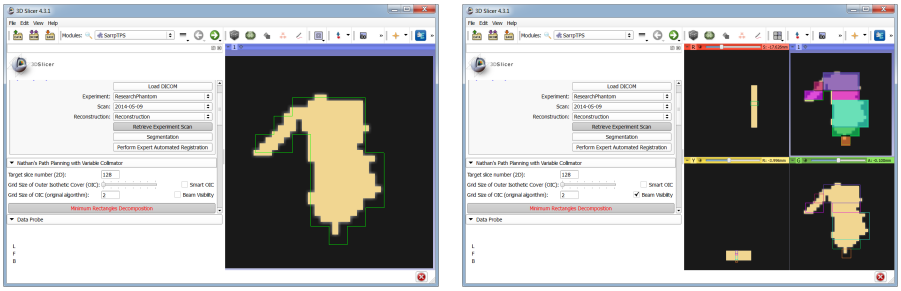

(a) OIC with a grid size of 3 (b) Decomposition with 7 rectangles

Fig. 4. An example of (a) OIC with a grid size of 3 and (b) its decomposition in SARRP TPS.

Decomposing the OIC into a minimum number of rectangles includes a series of processes including finding concave vertices from OIC points (note that concave vertices are a subset of OIC points), obtaining horizontal/vertical effective chords, building an intersection graph, running the Hopcroft-Karp algorithm,

decomposing the OIC using the resulting set, and running the PTR algorithm. Those decomposition steps are illustrated in Fig. 5.

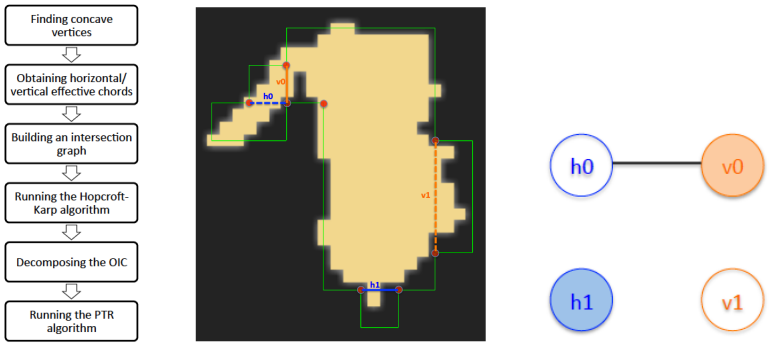

(a) Processes (b) Illustration (c) Intersection Graph

Fig. 5. (a) flow chart for decomposition steps. (b) shows 8 concave vertices represented by small dots in red; horizontal and vertical effective chords represented by dashed lines in blue and orange, respectively; h1 and v0 represented by solid lines are output of Hopcroft-Karp algorithm. The result of the PTR algorithm is shown in Fig. 4(b). (c) the intersection graph.

Each divided rectangle was represented as an instance of `vtkCubeSource` on the SARRP TPS and random RGB values were generated to associate a unique color to each rectangle for visualization purposes. The final result after the decomposition is shown in Fig. 4(b).

As a proof of concept, Fig. 6 depicts a representative dose volume for the example shape used in the previous figures. This dose volume was computed using the GPU-accelerated superposition-convolution method that has been integrated into the SARRP TPS, with a beam time of one minute for each rectangular shape. This is representative, and not necessarily accurate, because the variable collimator has not yet been commissioned. In particular, the computation used the fluence value of the 5×5 mm^2 collimator for all rectangular beams. Note that the size of largest rectangle, represented in green in Fig. 6(b), is 2.4×1.8 mm^2. This figure shows that higher dose occurs primarily at the boundaries between the rectangles, which will be a topic for investigation after commissioning is completed.

4 Conclusions and Future Work

In order to minimize the treatment time for dose painting of an arbitrary 2D shape, we have proposed an inverse planning pipeline to decompose the shape into the minimum number of rectangles for a given dimensional resolution. This introduces a tradeoff between accuracy and time, which the user resolves via a

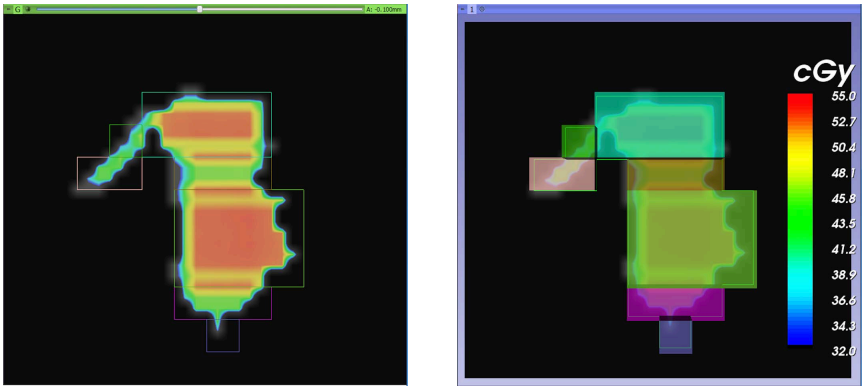

(a) Dose distribution (b) Dose distribution in 3D viewer

Fig. 6. Representative dose volume computed by SARRP TPS with a beam time of one minute for each rectangular region (not accurate because variable collimator has not yet been commissioned). (a) shows dose distribution in 2D cross-section, where CT and dose volumes were placed on foreground and background layers, respectively, and opacity of foreground layer was set to 50%. (b) shows 3D view with color bar indicating range of dose values.

slider bar that sets the grid size and graphically displays the resulting rectangular decomposition in the TPS. For a given rectangular decomposition, the GPU-accelerated dose engine can compute and display the resulting dose volume in a matter of seconds. Then, the modules available in SlicerRT [11], such as Dose Volume Histogram (DVH) and Isodose Contours, can be used to evaluate the treatment plan. Finally, the treatment plan can be delivered using the computer-controlled variable collimator developed for the SARRP.

Future work includes commissioning of the variable collimator, followed by testing of the dose painting experiments using EBT2 film. One specific issue will be the determination of the fluence rate for each collimator dimension, which is required by the GPU-accelerated dose engine. Currently, the fluence rate is determined for each collimator by scaling the computed dose to match the dose measured on film during commissioning. This is feasible for a small set of fixed-size collimators (e.g., 3×3 mm^2, 5×5 mm^2) but is not practical for a variable collimator. One approach is to interpolate between the two closest collimators (e.g., for 4×4 mm^2, given fluence values for 3×3 mm^2 and 5×5 mm^2). It is also likely that the fluence value will be proportional to the area of the collimator, at least when both dimensions are greater than a minimum value.

Also, the variable collimator currently includes a manual rotation, which could be motorized in the future. This would require the inverse planning method to be extended to consider rectangles of variable size and orientation.

Acknowledgments

This work has been supported by funding from Xstrahl Limited. SARRP was developed with support from NIH R01 CA108449.

References

1. Biswas, A., Bhowmick, P., Bhattacharya, B.B.: Construction of isothetic covers of a digital object: A combinatorial approach. Journal of Visual Communication and Image Representation 21(4), 295 – 310 (2010)
2. Boyer, A., Biggs, P., Galvin, J., Klein, E., LoSasso, T., Low, D., Mah, K., Yu, C.: Basic applications of multileaf collimators. Tech. Rep. 72, American Association of Physicists in Medicine (AAPM) (July 2001)
3. Cho, N., Kazanzides, P.: A Treatment Planning System for the Small Animal Radiation Research Platform (SARRP) based on 3D Slicer. In: MICCAI Workshop on Systems and Arch. for Computer Assisted Interventions (Oct 2012), http://hdl.handle.net/10380/3364
4. Ferrari, L., Sankar, P., Sklansky, J.: Minimal rectangular partitions of digitized blobs. Computer Vision, Graphics, and Image Processing 28(1), 58 – 71 (1984)
5. Gourley, K., Green, D.: A polygon-to-rectangle conversion algorithm. Computer Graphics and Applications, IEEE 3(1), 31–36 (Jan 1983)
6. Graves, E.E., Zhou, H., Chatterjee, R., Keall, P.J., Gambhir, S.S., Contag, C.H., Boyer, A.L.: Design and evaluation of a variable aperture collimator for conformal radiotherapy of small animals using a microCT scanner. Medical Physics 34(11), 4359–4367 (Nov 2007)
7. Hopcroft, J., Karp, R.: An $n^{5/2}$ algorithm for maximum matchings in bipartite graphs. SIAM Journal on Computing 2(4), 225–231 (1973)
8. Jacques, R., Wong, J., Taylor, R., McNutt, T.: Real-time dose computation: GPU-accelerated source modeling and superposition/convolution. Medical Physics 38(1), 294–305 (2011)
9. Matinfar, M., Iyer, S., Ford, E., Wong, J., Kazanzides, P.: Image guided complex dose delivery for small animal radiotherapy. In: Proc. IEEE Intl. Symp. on Biomedical Imaging (ISBI). pp. 1243–1246 (June 2009)
10. Pieper, S., Halle, M., Kikinis, R.: 3D slicer. In: Proc. of IEEE Internatinal Symposiuom on Biomedical Imaging. pp. 632–735 (April 2004)
11. Pinter, C., Lasso, A., Wang, A., Jaffray, D., Fichtinger, G.: SlicerRT – Radiation therapy research toolkit for 3D Slicer. Medical Physics 39, 6332–6337 (Oct 2012)
12. Stewart, J.M.P., Lindsay, P.E., Jaffray, D.A.: Two-dimensional inverse planning and delivery with a preclinical image guided microirradiator. Medical Physics 40(10) (2013)
13. Wong, J., Armour, E., Kazanzides, P., Iordachita, I., Tryggestad, E., Deng, H., Matinfar, M., Kennedy, C., Liu, Z., Chan, T., Gray, O., Verhaegen, F., McNutt, T., Ford, E., DeWeese, T.L.: High-resolution, small animal radiation research platform with x-ray tomographic guidance capabilities. International Journal of Radiation Oncology Biology Physics 71(5), 1591 – 1599 (2008)